Estimation of Airflow in Livestock Buildings

Rasmus Larsen
Institute for Mathematical Modelling
Technical University of Denmark, Building 321, DK–2800 Lyngby, Denmark
E–mail: rl@imm.dtu.dk, Phone: +45 4588 1433, FAX: +45 4588 1397

This work was supported by
Statens Jordbrugs- og Veterinærvidenskabelige Forskningsråd

Abstract

The well-being of the animals (e.g. pigs) in livestock buildings is contingent on adequate ventilation. Depending on the construction of the ventilation system draught may be introduced into the buildings. Obviously this is an unwanted effect, that might lead to decreasing growth of and increasing sickness among the livestock. Therefore it is of interest to estimate flow vector fields corresponding to the airflow introduced by a given ventilation system. By introducing particles (e.g. smoke or soapbubles) into the air-inlets of a model of a livestock building, the airflow in an laser-illuminated plane may be visualized. Based of sequences of images recorded of this plane local measurements of the velocity field are obtained by analysis of the local energy distribution, which is sampled using a set of 3-D spatio-temporal Gabor filters. We will show how physically inspired a priori distribution of the flow field may be used to integrate the local observations to a smooth field.

1 Introduction

Independently moving objects, rotation, dilation, shear in image sequences combine to produce complex velocity fields. Therefore, valid velocity estimation is restricted to local computations. This ensures that for sufficiently smooth velocity fields the estimation can be based on translational image velocity.

Coherent image translation is the basis for several computational methods. The main methods include correlation-based methods [21], differential methods [12, 18], energy-based methods [1, 10, 14] and phase-based methods [5, 4].

Restricting measurements to small spatio-temporal neighborhoods, however, often results in the measurements being based on one-dimensional intensity structures (edges and/or lines). In this case we can only determine the component of the velocity orthogonal to the intensity contour reliably. This is known as the aperture problem.

In general this problem exists in neighborhoods of the image sequence that have a one dimensional structure only, as well as neighborhoods that have no structure at all, that is in homogeneous areas. On the other hand, for image sequence neighborhoods that exhibit two dimensional spatial structures, such as intensity corners or various textured regions, we can reliably extract the true velocity. In order to identify the type of neighbourhood several approaches have been reported. In a correlation-based approach [2] used the curvature of the match surface, [18] investigated the use of second order spatial derivatives to identify the neighbourhood. The use of quadrature type filters tuned to different spatio-temporal frequencies has been used to identify the type of the neighbourhood in energy- as well as phase-based approaches [9, 4]

Because the aperture problem results in flow fields that are not fully constrained an assumption of smoothness of the velocity field must be applied in order to obtain a dense velocity field. One way of doing this is by applying a restriction that force the spatial derivatives to be small. These restictions are referred to as smoothness constraints [12]. Methods utilizing this type of smoothness constraints include the work of [18, 20, 16, 15]. Other approaches based on spatial filtering also have been reported. [19] for example used a vector median filter to obtain a smooth velocity field.

It is evident that local velocity estimation algorithms that are able to distinguish between the different natures of the neighborhood, and thus the estimated velocity - component velocity or not - should be more successful than algorithms that are not. In Section 3.1 we will shortly describe a method to extract velocity estimates as well as related directional certainties of the estimates based on the local energy distribution. This technique also will allow for the detection of unreliable results due to deviations from the assumption of coherent translational motion. This is especially important because of the distortion of features due to physical processes that can occur in fluids (e.g. [21]).

In Section 3.2 we will describe the implementation of the smoothness constraint. This smoothness constraint is formulated as a prior probability distribution for the velocity field that assigns high probability to fields that have small first order spatial derivatives, and low probability to fields that have large spatial derivatives. In particular we will concentrate on splitting the classic smothness constraint into physically interpretable terms as suggested by [13]. We will furthermore suggest an observation model that carefully relates the local estimates of normal velocity to a particular realization of the velocity field. Finally, we will combine the prior distribution and the observation model into a posterior distribution using Bayes' theorem.

2 Data

The algorithms described in this article will be applied to a sequence of images recorded at the Airphysics Laboratory at *Statens Jordbrugstekniske Forsøg*, Bygholm. The experiments are carried out in a 1:10 model of a segment of a livestock building. Using a laser sheet the airflow in a plane is illuminated. The smoke in the illuminated plane is recorded using a light sensitive videocamera.

3 Methods

This section is divided into two subsections. In Section 3.1 we will consider the local velocity estimation using a set of spatio-temporal directional quadrature filter pairs. After which in Section 3.2 we will formulate an algorithm for integrating these local estimates to a dense velocity field using smoothness constraints based on first order spatial derivatives of the velocity field.

3.1 Local Velocity Estimation

Because motion estimation in image sequences can be viewed as identification of patterns repeating themselves over time, it is natural to try to describe the motion analysis in the Fourier domain. Let us consider a neighbourhood containing a one dimensional intensity structure (e.g., a line) that translates coherently through time. In the spatio-temporal domain this corresponds to a neighbourhood of iso-grey level planes. Let these planes be given by their unit normal vector $\hat{\boldsymbol{k}} = (k_1, k_2, k_3)^T$. We will refer to this vector as the spatio-temporal orientation vector. The non-zero Fourier coefficents of this neighbourhood are concentrated to the line defined by $\boldsymbol{k}$. Furthermore the correspondence between this vector and the normal flow of the intensity structure is illustrated in Figure 1. The normal flow is given by

$$\boldsymbol{\mu} = (\mu, \nu)^T = \frac{-k_3}{k_1^2 + k_2^2}(k_1, k_2)^T \tag{1}$$

Now, in order to estimate this line, we will sample the Fourier domain using a set of spatio-temporal filters. Using a method developed by [14] this can be achieved by applying a set of directional quadrature filter pairs symmetrically distributed over the spatio-temporal orientation space. The directional quadrature filter pairs consist of a real even part and an odd imaginary part. The phase of the transfer function for the real part is shifted 90° relative to the imaginary part. By squaring and adding the two filter responses we obtain a phase independent estimate of the spectral density of the corresponding image structure.

In order to sample the Fourier domain we will employ a set of Gabor filters [7] tuned to frequencies distributed evenly across all spatio-temporal orientations, i.e. the center frequencies of the filters are the

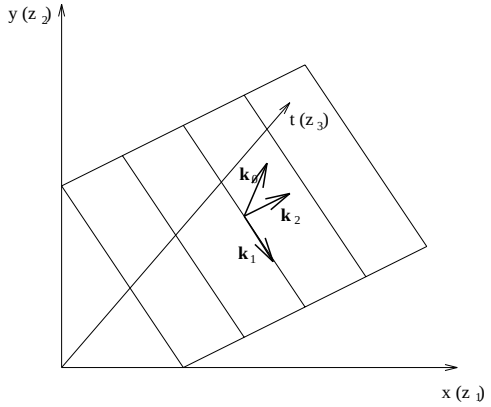

Figure 1: $\boldsymbol{k}$ is the unit normal vector of the iso-grey level planes generated by a translating line. $\boldsymbol{k}_1$ is the unit direction vector of the translating lines, and is therefore perpendicular to $\boldsymbol{k}$. $\boldsymbol{k}_2$ is a vector perpendicular to $\boldsymbol{k}$ as well as $\boldsymbol{k}_1$. The normal flow is found as the projection onto the (z_1, z_2) of $\boldsymbol{k}_2$ multiplied so its temporal coordinate equals 1.

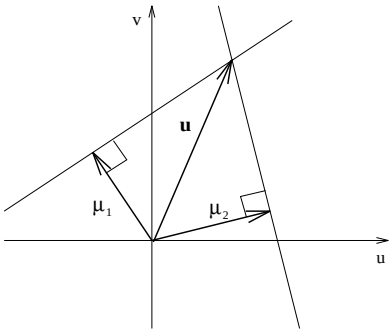

Figure 2: The true flow, $\boldsymbol{u}$, is constrained by the linear constraints given by the two normal flows, $\boldsymbol{\mu}_1$, and $\boldsymbol{\mu}_2$.

vertices of a diametrical symmetric regular polyhedron [14]. The pth Gabor filter consists of a Gaussian function shifted to the point $\boldsymbol{k}_p = (k_{p1}, k_{p2}, k_{p3})^T$ in frequency space. By dividing the filter into an odd and an even part we get the two transfer functions

$$Q_p^e(\boldsymbol{k}) = \frac{1}{(2\pi)^3}\left[\exp\left(\frac{(\boldsymbol{k}-\boldsymbol{k}_p)^2\sigma^2}{2}\right) + \exp\left(\frac{(\boldsymbol{k}+\boldsymbol{k}_p)^2\sigma^2}{2}\right)\right] \tag{2}$$

$$Q_p^o(\boldsymbol{k}) = \frac{1}{(2\pi)^3}\left[\exp\left(\frac{(\boldsymbol{k}-\boldsymbol{k}_p)^2\sigma^2}{2}\right) - \exp\left(\frac{(\boldsymbol{k}+\boldsymbol{k}_p)^2\sigma^2}{2}\right)\right] \tag{3}$$

The corresponding convolution masks are easily computed by taking the Fourier transforms

$$q_p^e(\boldsymbol{z}) = \frac{1}{(2\pi)^{3/2}\sigma^3}\cos(\boldsymbol{k}_p^T\boldsymbol{z})\exp\left(-\frac{\boldsymbol{z}^2}{2\sigma^2}\right) \qquad q_p^o(\boldsymbol{z}) = \frac{1}{(2\pi)^{3/2}\sigma^3}\sin(\boldsymbol{k}_p^T\boldsymbol{z})\exp\left(-\frac{\boldsymbol{z}^2}{2\sigma^2}\right) \tag{4}$$

Although Gabor filters are not quadrature pairs, they provide a reasonably good approximation for sufficiently small bandwidths [6]. If the bandwidth in octaves is measured at one standard deviation of the Gaussian envelope it is given by $B = \log_2[(\|\boldsymbol{k}\| + \sigma)/(\|\boldsymbol{k}\| - \sigma)]$.

Finally, the energy distribution of the Fourier domain as estimated by the set of quadrature filter pairs may be represented by the tensor $\boldsymbol{T} = \sum_p q_p \boldsymbol{n}_p \boldsymbol{n}_p^T$ where q_p is the output from the pth quadrature filter pair, and $\boldsymbol{n}_p$ is the unit normal vector defining the direction of the filter.

In order to find the direction of maximum spectral density we must find the unit vector $\boldsymbol{k}$ that maximizes $\boldsymbol{k}^T\boldsymbol{T}\boldsymbol{k}$. This vector is the eigenvector corresponding to the largest eigenvalue of $\boldsymbol{T}$. So for the coherently translating one-dimensional intensity structure, which has an effectively one dimensional Fourier domain, the spatio-temporal orientation vector is found by an eigen analysis of $\boldsymbol{T}$. Because the Fourier domain is one dimensional $\boldsymbol{T}$ has only one non-zero eigenvalue.

Now, if the translating structure has a two-dimensional intensity structure (e.g., a grey level corner) the spatio-temporal domain is described by two spatio-temporal orientations, giving rise to two non-zero eigenvalues of $\boldsymbol{T}$. The eigenvectors corresponding to these non-zero eigenvalues each translates into a normal flow by using Equation (1). These two normal flows each constrain the true flow in one direction as can be seen in Figure 2.

We can furthermore determine the perpendicular distance of the true flow to either of the constraint lines, this is given by

$$d_k(x_i, y_i) = \|(\boldsymbol{u}(x_i, y_i) - \boldsymbol{\mu}_k(x_i, y_i))^T \cdot \frac{\boldsymbol{\mu}_k(x_i, y_i)}{\|\boldsymbol{\mu}_k(x_i, y_i)\|}\|, \qquad k = 1, 2 \tag{5}$$

where $\boldsymbol{u}(x_i, y_i)$, $\boldsymbol{\mu}_k(x_i, y_i)$ are the true flow and the normal flows taken at the position (x_i, y_i).

It is the (weighted) sum of squares of these distances that should be minimized across the image in order to obtain the velocity field.

Deviation from the assumption of coherent translation, imperfectly designed filters and noise will result in non-zero Fourier coefficients not being contained in one single line or plane. In this case all three of the tensor eigenvalues will be non-zero. This allows us to extract information of the quality of the estimates of constraint lines we get from the eigenvectors corresponding to the two largest eigenvalues. Because imperfect conditions result in a non-zero third eigenvalue we suggest using a confidence measure for each of the linear constraints based on the difference of the corresponding eigenvalue and the least eigenvalue. Furthermore, a normalization of this difference should be made. This is evident as a noise free high step edge measures the motion just as well as a lower step does. We propose the following confidence measure for each of the linear constraints given by the eigenvectors corresponding to the two largest eigenvalues.

$$w_k(x_i, y_i) = \frac{\lambda_k(x_i, y_i) - \lambda_3(x_i, y_i)}{\lambda_k(x_i, y_i)}, \quad k = 1, 2 \tag{6}$$

Where $\lambda_1(x_i, y_i) \geq \lambda_2(x_i, y_i) \geq \lambda_3(x_i, y_i) \geq 0$ denote the eigenvalues of the tensor at position (x_i, y_i). This confidence measure approaches zero when the difference of the corresponding eigenvalue and the least eigenvalue approaches zero, and it attains its maximum value of one, when the least eigenvalue is zero, and the corresponding eigenvalue is the largest, or is equal to the largest eigenvalue, respectively.

3.2 Integration of local measurements

As mentioned in the Introduction we will apply an assumption of smoothness with the purpose of fully constraining the velocity field by forcing the spatial derivatives of the velocity field to be small. Since [12]'s original paper this has been investigated by several authors (e.g. [11, 17]). One way of formulating such a smoothness constraint is by use of Markovian random fields [8, 15]. We do this using the Bayesian paradigm. First we will formulate a prior distribution for the velocity field based on the spatial derivatives of the field.

Letting the flow at position (x_i, y_i), $i \in \{0, 1, \ldots, N-1\}$, be given by $\boldsymbol{u}(x_i, y_i) = (u(x_i, y_i), v(x_i, y_i))^T$ and the corresponding spatial derivatives be denoted by $\boldsymbol{u}_x(x_i, y_i) = (u_x(x_i, y_i), v_x(x_i, y_i))^T$ and $\boldsymbol{u}_y(x_i, y_i) = (u_y(x_i, y_i), v_y(x_i, y_i))^T$, the prior distribution of the flow field corresponding to the classical smoothness constraint of [12] may be described by a Gibbs distribution $p(\{\boldsymbol{u}\}) = \frac{1}{Z}\exp(-\beta U)$, where Z is a normalization constant and the energy term is given by

$$U' = \sum_{i=0}^{N-1} \left[\|\boldsymbol{u}_x(x_i, y_i)\|^2 + \|\boldsymbol{u}_y(x_i, y_i)\|^2 \right]. \tag{7}$$

where $\|\cdot\|$ is the Euclidean norm. This probability distribution assigns high probability to fields that exhibit small derivatives and low probability to field with high spatial derivatives. As shown by [13] by rearranging terms this energy function may be written

$$\begin{aligned} U' &= \frac{1}{2}\sum_{i=0}^{N-1}(u_x(x_i,y_i)+v_y(x_i,y_i))^2(\text{divergence}) \\ &+ \frac{1}{2}\sum_{i=0}^{N-1}(u_x(x_i,y_i)-v_y(x_i,y_i))^2+(u_y(x_i,y_i)+v_x(x_i,y_i))^2(\text{shear}) \\ &+ \frac{1}{2}\sum_{i=0}^{N-1}(u_y(x_i,y_i)-v_x(x_i,y_i))^2(\text{rotation}) \end{aligned} \tag{8}$$

Thus allowing us physically to interpret the smoothness constraint. Furthermore physical knowledge of the process in question may be built into the a priori model by weighting these three termes differently, i.e

$$U = \gamma_1 * (\text{divergence}) + \gamma_2 * (\text{shear}) + \gamma_3 * (\text{rotation}) \tag{9}$$

If for instance the two dimensional motion in question was due to solid body motion, we should choose an a priori distribution with a high γ_2, because shear should not occur in the field. Or if we were observing the two-dimensional flow of an incompressible fluid, we should choose a high γ_1, because the field would be divergence free.

Now if the spatial derivatives are implemented using these finite differences: $\boldsymbol{u}_x(x_i,y_i) = \boldsymbol{u}(x_i+1,y_i) - \boldsymbol{u}(x_i,y_i)$ and $\boldsymbol{u}_y(x_i,y_i) = \boldsymbol{u}(x_i,y_i+1) - \boldsymbol{u}(x_i,y_i)$. then the the energy function above can be implemeted using a second order neighbourhood.

Having constructed this prior distribution for the flow field we will now concern ourselves with an observation model. The observation relates the local observations or measurements of velocity to any particular realization of the prior distribution. This is done by a conditional Gibbs distribution

$$P(\boldsymbol{y}|\boldsymbol{u}) = \frac{1}{Z}\exp(-\alpha U_0) = \frac{1}{Z}\exp(-\alpha\sum_{i=0}^{N-1}\sum_{k=1}^{2} w_k(x_i,y_i)d_k(x_i,y_i)^2) \tag{10}$$

where $d_k(x_i,y_i)$ is the difference between the projection of the true flow onto the normal flow given by the kth eigenvector and the normal flow itself at pixel (x_i,y_i) as described by Equation (5). $w_k(x_i,y_i)$

is the certainty measure corresponding to this normal flow given by Equation (6). Z is a normalization constant. By using a Gibbs energy function that punishes larger deviation in the projection of the true flow onto the observed normal flows we allow smoothing in the direction not constrained by the normal flows while smoothing in the direction of the normal flow is punished. Furthermore the use of the confidence measures w_k derived in the previous section as weights allow us to take into consideration the quality of our measurements.

The prior distribution and the observation model are combined into a posterior distribution using Bayes' theorem. The energy function of the posterior distribution thus becomes

$$\begin{aligned} U &= \alpha \sum_{i=0}^{N-1} \sum_{k=1}^{2} w_k(x_i, y_i) d_k(x_i, y_i)^2 \\ &+\beta \sum_{i=0}^{N-1} \Big[\gamma_1 (u_x(x_i, y_i) + v_y(x_i, y_i))^2 + \gamma_3 (u_y(x_i, y_i) - v_x(x_i, y_i))^2 \\ &\qquad \gamma_2 ((u_x(x_i, y_i) - v_y(x_i, y_i))^2 + (u_y(x_i, y_i) + v_x(x_i, y_i))^2) \Big] \end{aligned} \tag{11}$$

In this energy function we can control the properties of estimated motion field. The faith in the observed or measured normal flows is controlled by α, the smoothness is controlled by β, and the modes of deformation of the field are controlled by γ_1, γ_2, and γ_3.

We can now apply a maximization scheme to the posterior distribution in order to obtain the maximum a posteriori estimate of the velocity field. This has been implemented using the Iterated Conditional Modes scheme by [3].

4 Results

As described in Section 3.1 we will represent the local Fourier domain by the energy tensor. We will use a set of ten Gabor filter pairs to sample the Fourier domain. The spatio-temporal directions of the Gabor filters are shown in Table 1 [9].

By setting the standard deviation of the Gaussian envelope equal to 1.5 and truncating the envelope at three standard deviations we arrive at the filter size, $11 \times 11 \times 11$. We set the bandwidth measured at one standard deviation to 1 octave. This results in a spatio-temporal frequency of the filters of 2. Since the Gabor filter kernels are separable [10] the 20 3-D convolutions may be performed by 140 1-D convolutions. Thus reducing the computational load by a factor 17.

Filter no.	1	2	3	4	6	7	8	9	10	
x	a	-a	b	b	0	0	-c	-c	-c	c
y	0	0	a	-a	b	b	c	c	-c	c
t	b	b	0	0	a	-a	c	-c	-c	c

Table 1: The spatio-temporal directions of the Gabor filters are given by these coefficients, where $a = 2/(10 + 2\sqrt{5})$, $b = (1 + \sqrt{5})/(10 + 2\sqrt{5})$, and $c = 1\sqrt{3}$.

Local estimates of normal flow are obtained by Gabor filtering and computation using Equation (1) on the smoke sequence. The computations are carried out on a spatially subsampled version of the image sequence. In order to remove unreliable measurements we have applied two threshholds. First, neighbourhoods of non-translational velocity are removed by only considering normal flows whose corresponding eigenvalue is at least twice as large as the smallest eigenvalues, i.e. $w_k > 0.5$, secondly by demanding that the local energy, i.e. the sum of the eigenvalues, exceeds 10 % of the maximum energy taking over the entire image we remove measurements of problematic signal-to-noise ratio.

To get a proper estimate of the velocity field, we will use the integration technique described in Section 3.2. Without loss of generality we may assume that the parameters of Equation (12) satisfies $\alpha+\beta = 1$, and $\gamma_1 + 2\gamma_2 + \gamma_3 = 1$.

In order to illustrate how weighting the three modes differently, we have estimated a series of flow fields corresponding to the image sequence shown in Figure 3(a) using different parameter settings. In Figure 3(b) equal weights has been used, whereas in Figures 3(c) and 3(d) rotation and divergence are punished five times as hard as the other modes of deformation, respectively.

Assuming that the air is approximately incompressible and the flow is two-dimensional, we would expect a model punishing divergence the hardest to yield the best fit to the data. This seems to be confirmed by the experiments. The field in Figure 3(d) is the most physically appealing.

5 Conclusion

By splitting the classical smoothness constraint into three physically interpretable terms, namely rotation, shear, and divergence, we have formulated a method for integrating local measurements of normal flow into a smooth flow field. Furthermore we have illustrated how physical reasoning may result in a more suitable model for the phenomenon at hand.

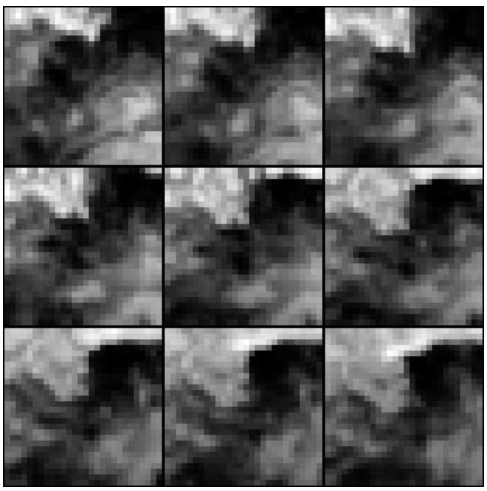

(a)

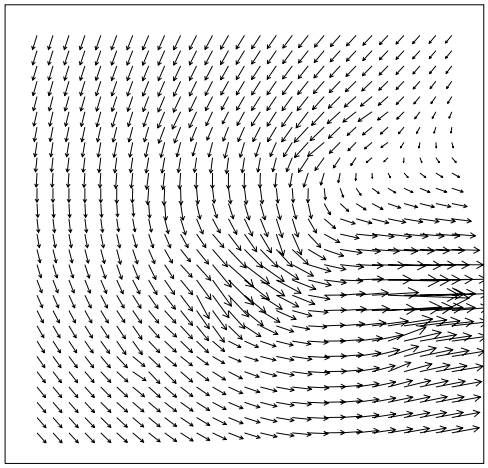

(b)

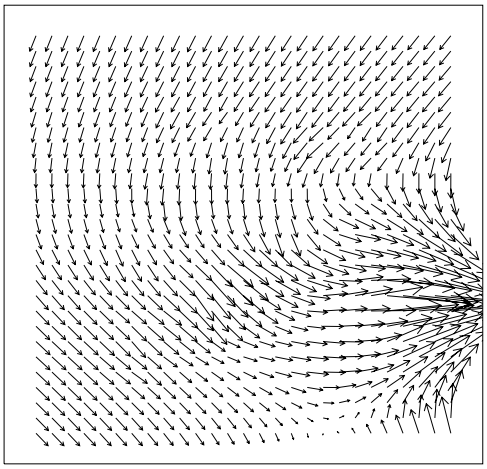

(c)

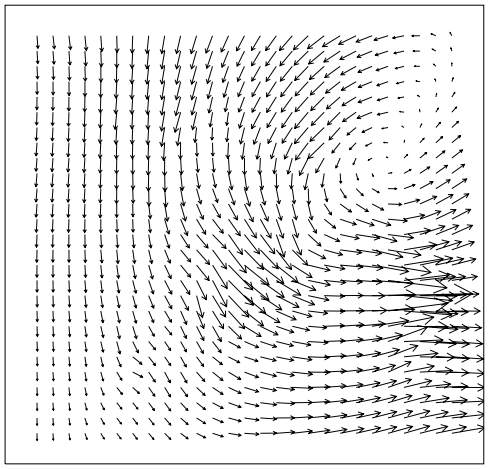

(d)

Figure 3: Sequence of images and estimated flow fields. (a) A subset of an image sequence, shown by row, recorded from a 1:10 scale model of a segment of a livestock building. The estimated flow field corresponding to the center image for (b) $\gamma_1 = 0.25$, $\gamma_2 = 0.25$, $\gamma_3 = 0.25$, i.e equal weights, (c) $\gamma_1 = 0.625$, $\gamma_2 = 0.125$, $\gamma_3 = 0.125$, i.e penalizing divergence five times as hard as rotation and shear, (d) $\gamma_1 = 0.125$, $\gamma_2 = 0.125$, $\gamma_3 = 0.625$, i.e penalizing rotation five times as hard as divergence and shear.

References

[1] Edward H. Adelson and James R. Bergen. Spatiotemporal energy models for the perception of motion. *Journal of the Optical Society of America, Series A*, 2(2):284–299, February 1985.

[2] P. Anandan. A computational framework and an algorithm for the measurement of visual motion. *International Journal of Computer Vision*, 2:283–310, 1989.

[3] Julian Besag. On the statistical analysis of dirty pictures. *Journal of the Royal Statistical Society, Series B*, 48(3):259–302, 1986.

[4] David J. Fleet. *Measurement of Image Velocity*. Kluwer Academic Publishers, Norwell, Mass., 1992. 203 pp.

[5] David J. Fleet and Allan D. Jepson. Computation of component image velocity from local phase information. *International Journal of Computer Vision*, 5(1):77–104, 1990.

[6] David J. Fleet and Keith Langley. Computational analysis of non-Fourier motion. Technical Report RPL–TR–9309, Robotics and Perception Laboratory, Department of Computing and Information Science, Queens University, Kingston, Ontario, Canada, 1993. 45 pp.

[7] Dennis Gabor. Theory of communication. *Journal of the Institution of Electrical Engineers*, 93:429–457, 1946.

[8] Stuart Geman and Donald Geman. Stochastic relaxation, Gibbs distributions and the Bayesian restoration of images. *IEEE Transactions on Pattern Analysis and Machine Intelligence*, 6(6):721–741, 1984.

[9] Leif Haglund. *Adaptive Multidimensional Filtering*. PhD thesis, Department of Electrical Engineering, Linköping University, Linköping, Sweden, 1992. 158 pp.

[10] David J. Heeger. Optical flow from spatio-temporal filters. In *First International Conference on Computer Vision*, pages 181–190, London, June 1987.

[11] Ellen Catherine Hildreth. Computations underlying the measurement of visual motion. *Artificial Intelligence*, 23:309–354, 1984.

[12] Berthold K. P. Horn and Brian G. Schunk. Determining optical flow. *Artificial Intelligence*, 17:185–203, 1981.

[13] Bernd Jähne. *Digital Image Processing.* Springer-Verlag, Berlin, Germany, 1991.

[14] Hans Knutsson. Representing local structure using tensors. In Matti Pietikäinen and Juha Röning, editors, *The 6th Scandinavian Conference on Image Analysis*, pages 244–251, Oulu, Finland, 1989. The Pattern Recognition Society of Finland.

[15] Janusz Konrad and Eric Dubois. Bayesian estimation of motion vector fields. *IEEE Transactions on Pattern Analysis and Machine Intelligence*, 14(9):910–927, September 1992.

[16] J. Marroquin, S. Mitter, and Tomaso Poggio. Probabilistic solution of ill-posed problems in computational vision. *Journal of the American Statistical Association*, 82:76–89, March 1987.

[17] Hans-Helmut Nagel. On the estimation of optical flow: Relations between different appoaches and some new results. *Artificial Intelligence*, 33:299, 1987.

[18] Hans-Helmut Nagel and Wilfried Enkelmann. An investigation of smoothness constraints for the estimation of displacement vector fields from image sequences. *IEEE Transactions on Pattern Analysis and Machine Intelligence*, 8(5):565–593, September 1986.

[19] James J. Simpson and Jason I. Gobat. Robust velocity estimates, stream functions, and simulated lagrangian drifters from sequential spacecraft data. *IEEE Transactions on Geoscience and Remote Sensing*, 42(3):479–493, May 1994.

[20] Demetri Terzopoulos. Regularization of inverse visual problems involving discontinuities. *IEEE Transactions on Pattern Analysis and Machine Intelligence*, 8(4):413–424, July 1986.

[21] Darrin D. Wahl and James J. Simpson. Physical processes affecting the objective determination of near-surface velocity from satellite data. *Journal of Geophysical Research*, 95:13511–16528, 1990.